Dynamics of Starburst Dendrimers

Zheng Yu Chen* and Chengzhen Cai

Department of Physics, University of Waterloo, Waterloo, Ontario, Canada N2L 3G1

Received January 7, 1999; Revised Manuscript Received May 19, 1999

ABSTRACT: We report the calculation of autocorrelation relaxation times, intrinsic viscosity, and the diffusion coefficient of a starburst dendrimer model, using both the preaveraging and variational-bound techniques. The model includes hydrodynamic effects, represented by the Rotne−Prager interaction, as well as excluded-volume repulsion, represented by a hard-core potential. Analytical derivations of the main formulae used in the paper are all explicitly given, and Monte Carlo simulations are used to carry out the thermodynamic average.

1. Introduction

1.1. General. Understanding the dynamical properties of macromolecules is important from both fundamental and practical perspectives. Figure 1 illustrates an ideal starburst dendrimer that has a uniformly and regularly branching structure. A basic repeating building block is termed a "spacer" and the total generation of a starburst molecule (G) is defined to be the number of spacers between the center of the molecule and any terminus. A significant difference between a dendrimer and a linear polymer in good solvents is the volume fraction within the molecule. The volume of a dendrimer is at most cubic in G, whereas the number of building units is exponential in G; thus even a single dendrimer is a densely packed system within itself.

The synthesis of starburst molecules was first reported in the early 1980s.[1] Since then, there have been a number of new synthetic techniques[2−7] based on modified or different approaches. The intrinsic viscosity ($[\eta]$), and other physical and chemical properties of dilute solutions of poly(amido amine) (PAMAM) dendrimers were measured in Tomalia's original work;[1] the NMR relaxation parameters of PAMAM dendrimers have been reported by Meltzer et al.,[2] who determined ^{13}C spin−lattice relaxation times (T_1), ^{2}H spin−lattice relaxation times (T_1), and spin−spin relaxation times (T_2). Another type of well-studied dendrimers is starburst polyethers (in both monodendron and tridendron forms),[5] whose intrinsic viscosity and hydrodynamic radius were recently measured by size exclusion chromatography. An interesting finding is that the hydrodynamic radius is approximately a linear function of G. More recently, Scherrenberg et al. conducted an extensive study of poly(propyleneimine) dendrimers up to five generations, using small-angle neutron scattering, viscosimetry measurements, and molecular-dynamics simulations.[6] They also found that the radius of gyration (R_g) is effectively linear in G and that the hydrodynamic radius (R_η) is related to R_g by $R_\eta \approx (^5/_3)^{1/2} R_g$. A series of carbosilane dendrimers of $G = 1-3$ with perfluorinated termini were studied recently by quasielastic neutron scattering. The static structure factor plots resemble those found in recent theoretical work.[7] The diffusion coefficient measured in this experiment will be compared to the theoretical results in this paper.

There are two major types of interactions that need to be considered in modeling the dynamical properties of dendrimer solutions: the excluded-volume interaction and the hydrodynamic interaction (there are also recent indications that electrostatic interactions may significantly change the conformation of dendrimers[8]). In this paper, we examine the applicability of conventionally used approaches in statistical physics that incorporate these interactions for the study of dendrimer dynamics. In particular, we examine the dynamic relaxation times and the transport properties of a "standard" bead−bond model that has been exclusively studied for its conformational properties.

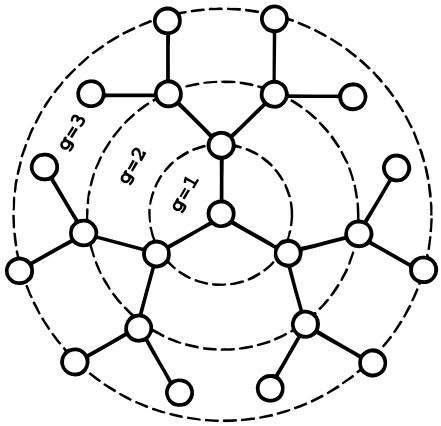

Figure 1. Sketch of a three-generation dendrimer model. The circles represent hard beads with diameter d and the solid lines represent rigid rods with length a, which can freely rotate about the branching joints. Note that this structure is defined as a two-generation dendrimer in some literature.

Readers who are not interested in technical details may skip directly to subsections 2.5 and 3.3, which contain the main results and a comparison with experimental measurements. The paper is organized as follows: in the rest of this section, a literature review of existing efforts in theoretical modeling of dendrimers will be given; in section 2, a Zimm preaveraging approximation will be introduced, and the calculation for the longest correlation times of dendrimers will be reported; and in section 3, the transport properties, i.e., the intrinsic viscosity $[\eta]$ and diffusion coefficient D, will be examined by using various approximate methods. Appendix A is a short mathematical account of the eigenproblem encountered in section 2, and Appendix B contains brief steps leading to the Fixman variational bounds for both $[\eta]$ and D used in section 3.

1.2. Literature Review. The earliest theoretical study of the configurational properties of starburst

10.1021/ma990018y CCC: $18.00
Published on Web 07/20/1999

dendrimers can be found in de Gennes and Hervet's work, where a simple mean-field model was developed.[9] The density profile was found to increase monotonically outward from the center of the molecule, and the critical generation was predicted to be proportional to the logarithm of the spacer length. However, there are a few deficiencies in their model, as the assumptions that all segments in the same generation lie in the same shell about the branching center and that all branches stretch outward were recently shown to be unrealistic in various numerical simulations.[10−12] Another self-consistent mean-field model and a scaling argument were considered more recently by Boris and Rubinstein.[13] They have examined the conformational properties in the weak-density region where the excluded-volume interaction can be modeled effectively by a second virial term. Many of their conclusions agree well qualitatively with simulation results and disagree with those drawn from the de Gennes−Hervet mean-field model.

The first set of computer simulations of a course-grained model were based on a *kinetic* growth algorithm,[10] where dendrimers were modeled as strings of beads, as shown in Figure 1, that can be grown from a central core. Such a dendrimer model is characterized by the functionality (f) of the branching units, the total generation (G), and the number of monomers (P) in each spacer ($f = 3$ and $P = 1$ in Figure 1). The total number of monomers is thus given by $N + 1$ where $N = Pf[(f - 1)^G - 1]$, which grows exponentially as G increases. In contrast to de Gennes−Hervet's results, Lescanec and Muthukumar found that the density profiles decrease monotonically outward from the branching center and that there exist significant back-folding branches. The dimensions of the molecule were found empirically to be proportional to $N^{\nu}P^{\beta}$, with $\nu = 0.22 \pm 0.02$ and $\beta = 0.50 \pm 0.02$. On a diamond lattice Mansfield and Klushin performed equilibrium Monte Carlo simulations, which showed similar overall density profiles.[11] They suggested that the central core region is probably less dense due to strong outward stretching demands of the initial few generations. Using an equilibrium pivot algorithm in free space, Chen and Cui systematically performed Monte Carlo simulations in different density regimes for a bead−bond model with various P and G.[12] When the excluded-volume effects are relatively weak, they found that the dimension of the molecules follows an empirical scaling law $(PG)^{1-\nu}N^{2\nu-1}$ where $\nu = 0.589$ is the Flory exponent, thus confirming an early general theoretical conclusion that the conformational properties of regularly branched polymers belong to the universality class of linear polymers.[14] In the dense regime, however, the scaling law breaks down. The critical generation found is in accordance with the de Gennes−Hervet prediction, which can actually be obtained by a simple maximum-packing argument. Recently, Welch and Muthukumar have investigated the density profile of dendritic polyelectrolytes in solution and have found that a reversible transition between the dense-core and dense-shell structures exists when the ionic strength of the solvent varies from low to high.[8]

There exist several theoretical approaches in studying the dynamical properties of linear and star polymers. Early considerations can be traced back to a Kirkwood paper, where the method of pre-averaging in the hydrodynamic tensors was first suggested.[15] The formulae for calculating transport coefficients were given explicitly, on the basis of various approximations that were later improved. The Brownian diffusion of macromolecules in solvent was analytically treated by Rouse, who studied a simple molecular model that contains neither excluded-volume nor hydrodynamic interactions.[16] Later, Zimm devised a preaveraging method, together with other approximations, and studied linear polymer models incorporating both excluded-volume and hydrodynamic interactions.[17] A similar method was also applied to the study of the dynamics of star polymers, the simplest type of branching polymers, which resemble linear polymers rather than the hyperbranching polymers with complicated structures found decades later.[18] It is relatively easy to treat the Langevin equation of linear polymers because of the simplicity in linear-polymer architecture that makes mapping into a continuous notation possible. Such a "luxury" does not exist for the study of hyperbranching polymers.

Modern computers enable us to directly simulate macromolecular dynamics without making any mathematical approximations.[19−21] A comprehensive review can be found in a recent book.[22] The simulations that include hydrodynamic interactions, however, are often limited to relatively small macromolecules due to limitations of computer power.

For dendrimers, molecular-dynamics simulations with atomic-level potential energies were carried out only for hundreds of picoseconds.[23] Since the correlation times of starburst dendrimers are usually in the range of microseconds, these simulations probably never reached thermal equilibrium. Nevertheless, the simulated molecules showed rather open structures without any indication of the shell structure proposed in de Gennes and Hervet's work. Molecular-dynamics simulations were also recently performed on a more abstract model, where a soft potential energy between the monomers was used to determined the radius of gyration and the relaxation times.[24] No hydrodynamic interactions were considered in these simulations.

Applying Lescanec and Muthukumar's algorithm, Mansfield and Klushin calculated the static scattering factor and the hydrodynamic radii for a bead−bond model with an excluded-volume interaction represented by a bead size of $d = {}^{5a}/_{6}$ where a is the effective bond length between the adjacent units.[11,27] The experimental hydrodynamic radii of PAMAM dendrimers were also compared with the computed variational bounds for a $P = 2$ dendrimer model.[27]

Recently, La Ferla[25] and Cai and Chen[26] proposed analytical approaches to study the dynamics of dendrimer models. La Ferla calculated the radii of gyration (R_g), hydrodynamic radii (R_η), static structure factors, and the first cumulant of the dynamic structure factor, where the hydrodynamic effects were examined without the inclusion of an excluded-volume interaction. The static structural factors, R_g and R_η, qualitatively agree with the results of Mansfield and Klushin, despite of the lack of excluded-volume interactions in his model. In our recent work, normal-mode displacements of the monomers in a Rouse approximation (without excluded-volume and hydrodynamic interactions) were classified. The high degeneracy of the normal modes was studied analytically and is consistent with La Ferla's numerical calculations. The relaxation time can be shown to be proportional to G for large G, and the intrinsic viscosity is approximately a linear function of G.[26]

In this paper, we report new analytical treatments of the dynamical properties based on the same bead−bond model used earlier by one of us.[12] Both excluded-volume and hydrodynamic interactions are effectively included in the calculation. Our interest lies in the high-density regime where the nonuniversal behavior is more profound and is not well understood theoretically. Both Zimm's preaveraging and Fixman's variational approximations will be examined.

2. Preaveraging Approximation

2.1. Basic Equations. Consider a polymer that is modeled by a system of $N + 1$ connected spherical particles with identical diameter d, moving in a solvent environment. Because of the presence of the solvent molecules, the force acting on the kth particle may have a solvent-mediated effect on the jth particle, depending on the distance vector between them. One assumes that the velocity of the jth particle has the form

$$\mathbf{v}_j = \frac{1}{\zeta}\sum_k \mathbf{H}_{jk}\cdot\mathbf{W}_k \quad (j \text{ and } k = 0, ..., N) \tag{2.1}$$

where $\mathbf{W}_k$ is the total force acting on the kth particle, and $\mathbf{H}_{jk}$ is the hydrodynamic interaction tensor between the jth and kth particles. The Langevin equation, which is customarily used to describe the time-dependent dynamic motion of the system, is an equation with $N_f = 3(N + 1)$ degrees of freedom[28]

$$\frac{\mathrm{d}}{\mathrm{d}t}\mathbf{r}_j = \sum_{k=0}^{N}\frac{1}{\zeta}\mathbf{H}_{jk}\cdot[-\nabla_k U + \mathbf{f}_k(t)] \quad (j, \text{ and } k = 0, ..., N) \tag{2.2}$$

where $\mathbf{f}_k(t)$ is the Brownian force acting on particle k and U is the intramolecular interaction potential depending on the position vectors of all particles. Usually the random forces assume a Gaussian type

$$\langle\mathbf{f}_j(t)\rangle = 0 \quad (j = 0, ..., N)$$

$$\langle\mathbf{f}_j(t)\mathbf{f}_k(t')\rangle = 2k_\mathrm{B}T\zeta\mathbf{H}_{jk}^{-1}\,\delta(t - t') \quad (j \text{ and } k = 0, ..., N)$$

where $\mathbf{H}_{jk}^{-1}$ is a tensor satisfying $\sum_k \mathbf{H}_{jk}^{-1}\cdot\mathbf{H}_{kl} = \delta_{kl}\mathbf{I}$. We may construct a matrix $\mathbf{H}$, whose (j, k)th block is the tensor $\mathbf{H}_{jk}$, to represent the overall dynamics of the entire system.

There exist two commonly used approximations for $\mathbf{H}_{jk}$: the Oseen tensor[28] and the Rotne−Prager tensor.[29] The former represents the hydrodynamic effect between two infinitesimal, pointlike particles, which can be expressed as

$$\mathbf{H}_{jk} = \begin{cases}\dfrac{3d}{8r_{jk}}(\mathbf{I} + \hat{\mathbf{e}}_{jk}\hat{\mathbf{e}}_{jk}) & (j \neq k)\\ \mathbf{I} & (j = k)\end{cases} \tag{2.3}$$

where $\mathbf{r}_{jk} = |\mathbf{r}_{jk}| = |\mathbf{r}_j - \mathbf{r}_k|$ is the distance between two particles labeled j and k, and $\hat{\mathbf{e}}_{jk}$ is a unit vector along the direction of vector $\mathbf{r}_{jk}$. This simple form basically demonstrates that the hydrodynamic interaction has a screening effect following r^{-1} behavior. However, when two particles are close enough, it suffers from the problem that $\mathbf{H}$ is not positive-definite. Physically, the Oseen tensor fails to describe the properties of finite-size particles at a small scale. This problem was later resolved by Rotne and Prager, who used a variational method to minimize the energy dissipation rate in a solvent and thus guaranteed the positive definiteness of $\mathbf{H}$. The Rotne−Prager tensor has the form

$$\mathbf{H}_{jk} = \begin{cases}\dfrac{3d}{8r_{jk}}\left[\left(1 + \dfrac{d^2}{6r_{jk}^2}\right)\mathbf{I} + \left(1 - \dfrac{d^2}{2r_{jk}^2}\right)\hat{\mathbf{e}}_{jk}\hat{\mathbf{e}}_{jk}\right] & (j \neq k)\\ \mathbf{I} & (j = k)\end{cases} \tag{2.4}$$

and is widely used in more recent treatments.[22,28] Due to the drawbacks of the Oseen tensor, we use the Rotne−Prager tensor throughout this paper.

In the so-called free-draining limit, when the solvent molecules can be ignored or when the size of monomers is much smaller than the bond length, $\mathbf{H}_{jk}$ is reduced to a 3×3 zero matrix when $j \neq k$. In such cases, the terms associated with the hydrodynamic interaction in eq 2.2 are decoupled, and the only coupling source comes from the spatial dependence in U, as the right-hand side of eq 2.2 shows.

Going back to the general consideration of eq 2.2, we must deal with spatially dependent hydrodynamic tensors. The frequently used "preaveraging method" is a procedure which replaces the $\mathbf{H}$ matrix by its thermodynamic average, as originally proposed by Zimm.[17] It is easy to verify that the averaged versions of both Oseen and Rotne−Prager tensors share the same expression

$$\langle\mathbf{H}_{jk}\rangle \equiv H_{jk}\mathbf{I} = \begin{cases}\left\langle\dfrac{\mathrm{d}}{2r_{jk}}\right\rangle\mathbf{I} & (j \neq k;\ j, k = 0, 1, ..., N)\\ \mathbf{I} & (j = k)\end{cases} \tag{2.5}$$

One advantage of the Zimm approximation is that the hydrodynamic matrix $\mathbf{H}$ is now a constant, and one can employ similar theoretical approaches developed for the free-draining limit.

In a more exact treatment of the Brownian dynamics, Ermark and McCammon solved the Langevin equation numerically by explicitly including the spatially dependent hydrodynamic tensors.[19] They found that the Oseen tensor does not always guarantee a positive-definite $\mathbf{H}$, which results in failure to generate random forces, because a covariance matrix is mathematically required to be positive-definite. They also found that, even when such a problem does not occur, there could be a significant difference between the results obtained from the use of Oseen tensors and Rotne−Prager tensors.

The intramolecular interaction potential U generally includes the excluded-volume interaction between monomers, represented by the diameter d, and the chemical-bonding effect between adjacent monomers. The simplest case is the Rouse model, where the excluded-volume interaction is disregarded. Since the size of the monomers is effectively treated as zero, the configurations of a linear polymer chain can be modeled as random walks in three-dimensional space, which can be equivalently modeled by a string of N successively linked identical springs. For example, the interaction potential between the jth monomer and the $(j + 1)$th monomer can be expressed as $3k_\mathrm{B}T(\mathbf{r}_j - \mathbf{r}_{j+1})^2/a^2$, where a is the effective bond length. In this case, the Langevin equations describe the temporal evolution of a set of linearly coupled random variables, which is sometimes

termed an Ornstein−Uhlenbeck process and is analytically solvable. Following the prescribed procedure of solving linear differential equations, one can define normal coordinates to characterize the linearly independent motions of the system. The temporal correlation of each normal coordinate assumes an exponential function, whose decay rate is the inverse of the corresponding eigenvalue of the coefficient matrix of this linear system. Thus, all dynamical information of the system becomes available once the eigensystem of the coefficient matrix is solved. For linear polymers, this procedure is straightforward.[16,17] For polymers with other types of architectures, such as stars, the computation is usually more involved.[18] Recently, we have discussed dendrimer dynamics based on a Rouse approximation.[26]

2.2. Ornstein−Uhlenbeck Process. Under the preaveraging approximation, the subject of interest in this section, each $\mathbf{H}_{jk}$ is reduced to a constant tensor $H_{jk}\mathbf{I}$. In order to deal with the general problem of incorporating the long-rang interactions, particularly the excluded-volume interaction, into the formalism, we approximate the potential energy U in a quadratic form

$$U = \frac{K}{2}\sum_{j=1}^{N}\sum_{k=1}^{N}(\mathbf{r}_j - \mathbf{r}_0)\cdot\mathbf{A}^*_{jk}\cdot(\mathbf{r}_k - \mathbf{r}_0) \qquad (2.6)$$

where $K = 3k_BT/a^2$ and $\mathbf{A}^*_{jk}$'s are the force matrices. The potential has been written with respect to a reference vector $\mathbf{r}_0$, which guarantees the translational invariance of U. Although 0 is the label of the central core according to our current notation, it could also be the label of an arbitrary monomer.

Mathematically, U has a form similar to that in the Rouse model, but conceptually, we stress that the effective force matrices $\mathbf{A}^*_{jk}$ are now a combination of both excluded-volume interactions and the chemical bonding that determines the architecture of the molecule. In view of the symmetry of the space, $\mathbf{A}_{jk} = A_{jk}\mathbf{I}$; thus, the three Cartesian directions can be treated equally. The force matrices are determined by the classical equipartition theorem: since the potential is quadratic in coordinates, we expect

$$a^2K\sum_k \mathbf{A}^*_{jk}M_{kl} = k_BT\delta_{jl} \qquad (2.7)$$

where

$$M_{jk} = (1/3a^2)\langle(\mathbf{r}_j - \mathbf{r}_0)\cdot(\mathbf{r}_k - \mathbf{r}_0)\rangle \qquad (2.8)$$

and $\langle\cdot\rangle$ represents the thermodynamic average. In a matrix form, $A^* = (A^*_{jk})$ is the inverse of the matrix $M = (M_{jk})$. The evaluation of the M matrix itself, however, depends on the concrete statistical-physics models adopted for the conformational properties.

We have used the same numerical procedure as elsewhere[12] to perform the average in eqs 2.5 and 2.8. Normally, a few million Monte Carlo pivot moves were attempted for each case, which produces the force matrix within a relative error smaller than 0.1%. A high-precision numerical procedure was used in performing the matrix inversion of A in eq 2.7.

In matrix notation, the Langevin equations are then simplified to

$$\frac{\mathrm{d}}{\mathrm{d}t}\mathbf{r} = \frac{1}{\zeta}\mathbf{H}[-K\mathbf{A}\mathbf{r} + \mathbf{f}] \qquad (2.9)$$

where the conformation of the molecule is represented by an $N_f \times 1$ column matrix $\mathbf{r}$, whose $(3j+1)$th to $(3j+3)$th elements are the three Cartesian components of vector $\mathbf{r}_j$ with $j = 0, ..., N$, and $\mathbf{f}$ is the random force matrix arranged in the same way and characterized by the first two cumulants

$$\langle\mathbf{f}(t)\rangle = 0 \qquad (2.10)$$

$$\langle\mathbf{f}(t)\mathbf{f}^{\mathrm{T}}(t')\rangle = 2k_BT\zeta\mathbf{H}^{-1}\delta(t - t') \qquad (2.11)$$

Now, since each block of the force matrix $\mathbf{A}$ is expressed as $\mathbf{A}_{jk} = A_{jk}\mathbf{I}$

$$A_{00} = \sum_{j=1}^{N}\sum_{k=1}^{N}A^*_{jk} \qquad (2.12)$$

$$A_{0j} = A_{j0} = -\sum_{k=1}^{N}A^*_{jk} = -\sum_{k=1}^{N}A^*_{kj} \quad (j = 1, ..., N) \qquad (2.13)$$

$$A_{jk} = A^*_{jk} \quad (j, k = 1, ..., N) \qquad (2.14)$$

As is evident from eq 2.9, the mathematical problem finally becomes how to solve the eigensystem of matrix HA. Similar treatments can be found elsewhere.[17,18,25]

2.3. Normal Modes and Their Decay Rates. As discussed in the previous subsection, the normal modes and their corresponding eigenvalues are important for the description of the collective motion of monomers in the solvent and their dynamic decay rates. We concentrate on solving the eigensystem of the matrix HA in this section.

Generally speaking, HA is a dense, asymmetric matrix, which can be analytically diagonalized only in very special cases. Since the labels of the monomers are no longer continuously ascending as in linear polymers, we must diagonalize the matrix with a discrete notation. Even in the simplest case of the Rouse approximation, A is a sparse matrix that can be diagonalized only semianalytically.[26] For the θ temperature Zimm model,[25] the eigenvalues of HA were numerically computed for various adjustable system parameters by La Ferla, whereas the normal-mode displacements were not determined. In this work, we consider both excluded-volume and hydrodynamic interactions for dendrimer models; thus, both A and H are nontrivial. The eigenvalues can be numerically computed through the use of the QR decomposition.[30,31]

In Figure 2, we show the eigenspectrum of the HA matrix for a $G = 6$ dendrimer with various squared excluded-volume diameters, $d^2 = 0.99a^2$, $0.5a^2$, and $0.1a^2$. The vertical axis shows the scaled decay rate, i.e., $1/\lambda$, in logarithmic scale, and the horizontal axis shows the index of eigenvalues. There is always an exact eigenvalue, 0, which is not included in the figures but will be discussed in the next subsection. The three plots display a similar pattern, which suggests that apart from the shift in the numerical values, the structure of the eigenvalues, including the descending order of the magnitudes, remains basically the same as in a Rouse approximation.[26] A further comparison between these plots and La Ferla's eigenspectrum,[25] which is based on a completely different interaction potential, indicates

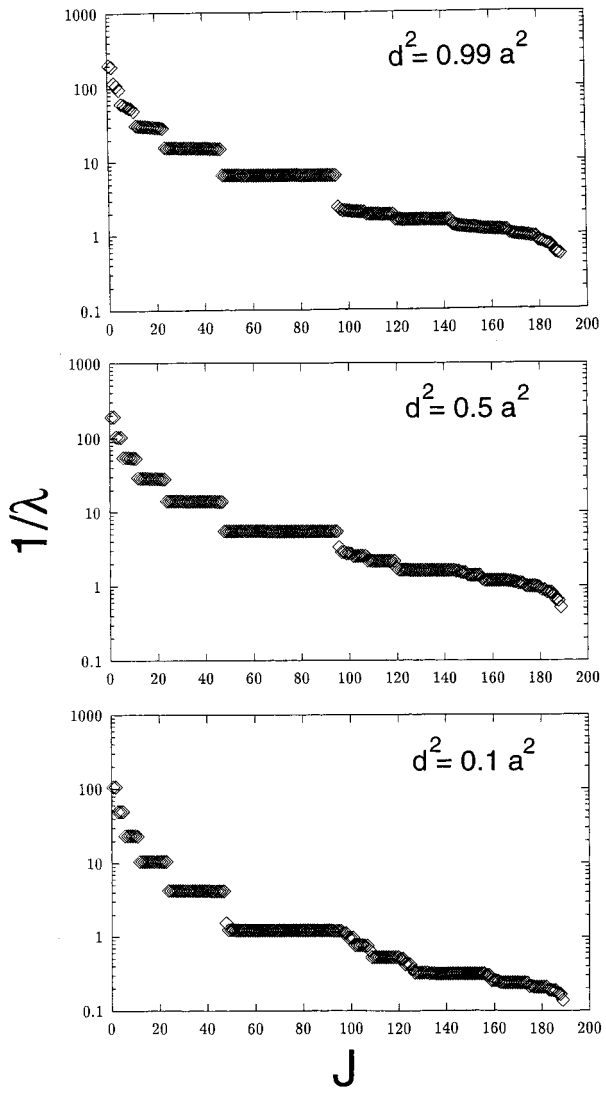

Figure 2. Spectra of relaxation rates for $G = 6$ dendrimer models with different bead size. The horizontal axis shows the index of the eigenvalues arranged so that the eigenvalues are in ascending order.

the same qualitative behavior too. The most important eigenvalues will be discussed in subsection 2.5.

Due to the high degree of degeneracy, many values of the eigenvalues are very close to each other; however, they are not exactly equal because of the numerical errors introduced by the Monte Carlo procedure. Thus, the degree of degeneracy cannot be determined from the numerical results alone. La Ferla has listed the degeneracy of some eigenvalues without rigorous mathematical proof. In our previous work, the eigenvectors were analyzed and classified into two main categories in a Rouse approximation.[26] By carefully treating the symmetry properties of matrices H and A in the current model analytically, we have arrived at the conclusion that the same classification is also applicable to the Zimm approximation; the procedure is detailed by Cai[32] and will not be repeated here. The readers may refer to Cai and Chen[26] for the discussions of the eigenvalues and -vectors.

2.4. Drifting Mode. It is worth noting that $\lambda_0 = 0$ is always an eigenvalue corresponding to an eigenvector $\iota = (1, 1, ..., 1)^T$, which physically means that all the monomers have a common displacement, i.e., a pure translational motion. This is based on the fact that U is a translational invariant, which implies $\sum_k \nabla_k U = 0$ and leads directly to

$$\sum_k A_{jk} = \sum_k \frac{\partial^2 U}{\partial r_{j\mu} \partial r_{k\mu}} = \frac{\partial}{\partial r_{j\mu}} \left(\sum_k \frac{\partial U}{\partial r_{k\mu}} \right) = 0 \quad (2.15)$$

or $A\iota = 0$ thus $HA\iota = 0$.

Physically, if one multiplies both sides of the Langevin equation (A.1) by H^{-1}, it is clear that it describes a system with a mass matrix H^{-1},

$$\frac{\mathrm{d}}{\mathrm{d}t} H^{-1} r = \frac{1}{\zeta}(-KAr + f) \quad (2.16)$$

The drifting center

$$\mathbf{r}_C = \frac{\sum_{jk} (H^{-1})_{jk} \mathbf{r}_k}{\sum_{jk} (H^{-1})_{jk}} \quad (2.17)$$

is the effective center of mass of the new system and should not be mistaken for that of a static molecule. When dynamical properties are considered, it is this drifting center that should be considered as a reference center.

2.5. Correlation Functions and Relaxation Times. For convenience, we shall arrange the eigenvalues of the HA matrix in ascending order

$$0 = \lambda_0 < \lambda_1 \leq ... \leq \lambda_N \quad (2.18)$$

and the eigenvectors and the general coordinates x_j's will be rearranged accordingly. Solving the Langevin equation (A.5) for each $x_j(t)$ individually and incorporating the properties of the fluctuating Brownian forces $\mathbf{f}(t)$, one arrives at[28]

$$\langle x_j(t) x_k(0) \rangle = (k_B T/\lambda_j K) \delta_{jk} \exp(-t/\tau_j) \quad (2.19)$$

where j and $k \neq 0$, and $\tau_j = \zeta/\lambda_j K$. Therefore, within a trivial coefficient, $1/\lambda_j$ characterizes the decay time for the jth normal mode fluctuation.

One of the most important measures for dynamic relaxation is the autocorrelation for the monomer-to-center vector

$$\mathbf{Q} = \mathbf{r}_q - \mathbf{r}_0 \quad (2.20)$$

where q is the label of an arbitrary monomer. The autocorrelation function of $\mathbf{Q}$ defines the rotational relaxation time τ_r in the large-t limit,

$$\langle \mathbf{Q}(t) \cdot \mathbf{Q}(0) \rangle \propto \exp(-t/\tau_r) \quad (2.21)$$

Another measure of practical interest is the autocorrelation function of the squared radius of gyration

$$R_{gy}^2 = \frac{1}{N+1} \sum_{j=0}^{N} (\mathbf{r}_j - \mathbf{r}_c)^2 \quad (2.2)$$

where $\mathbf{r}_c$ is the position vector of the center of mass of the molecule. The autocorrelation function of R_{gy}^2 characterizes radial elastic motion and defines the elastic relaxation time τ_e in the large-t limit,

$$\langle R_{gy}^2(t) R_{gy}^2(0) \rangle - \langle R_{gy}^2 \rangle^2 \propto \exp(-2t/\tau_e) \quad (2.23)$$

Table 1. Relaxation Times Calculated from a Preaveraging Approximation for Our Dendrimer Models with Different Bead Sizes and Generations[a]

	$d^2 = 0.99a^2$		$d^2 = 0.5a^2$		$d^2 = 0.1a^2$	
G	τ_r	τ_e	τ_r	τ_e	τ_r	τ_e
1	1.846	1.846	1.585	1.592	1.187	1.187
2	5.761	5.761	5.037	5.041	4.107	4.107
3	13.93	13.93	12.37	12.38	10.38	10.40
4	30.31	30.31	27.31	27.23	23.21	23.25
5	62.78	62.85	56.55	56.52	49.33	49.34
6	127.8	127.8	113.4	113.4	102.2	102.4
7					204.4	204.4

[a] Both τ_r and τ_e are expressed in units of $a^2\zeta/3k_BT$.

In a preaveraging approximation, such as the one adopted in this section, all correlation functions can be expressed as a summation of the autocorrelation functions of the normal modes. One can show that in the large time scale the normal mode with the slowest decay rate is most important, provided that (a) there is no high degree of degeneracy of the next slowest decay time and (b) the numerical coefficients associated with higher modes do not diverge; thus, the relaxation times are

$$\tau_r = \tau_e = \tau_1 = \zeta/\lambda_1 K \tag{2.24}$$

Table 1 lists the relaxation times for various parameters in our dendrimer model. The computation of τ_e was carried out by searching through the list of eigenvalues found in the previous section. The computation of τ_r, was based on a different technique, the power method, which is a more precise and efficient method for calculating the dominating eigenvalue. Both methods produce the same results within the range of numerical error.

We have previously concluded that $\tau_e = \tau_r$ for a dendrimer model in the Rouse approximation. In the current work, we have included both excluded-volume and hydrodynamic interactions, and the same conclusion still stands. This is not unexpected in a linearized version of the Langevin equations because of the fact that any long-time motion is governed by the slowest decay rate. Grest and coworkers have examined the dynamics of star polymers via molecular dynamics and have found $\tau_e < \tau_r$.[22,24] In practical dendrimer systems, τ_e should be smaller than τ_r as well. The conclusion of $\tau_e = \tau_r$ is an artifact, and these two relaxation times should be separable in a theory that goes beyond the linearization treatment.

An interesting scaling relation for any macromolecule is

$$\tau_r D \propto \langle R_{gy}^2 \rangle \tag{2.25}$$

which simply states that, during a time τ_r, the center of mass diffuses through a distance approximately equal to the average size of the molecule. Linear polymers and star polymers, for example, obey this scaling relation, as previously demonstrated by Doi and Edwards[28] and Grest and coworkers.[35] Using τ_r computed here and the values of D calculated in the next section, we have plotted $\tau_r D/\langle R_{gy}^2 \rangle$ for various G's and d's in Figure 3. As can be seen from this figure, this ratio approaches a constant as G increases for modest d^2. The deviation at large G for $d^2 = 0.99a^2$ is an indication that the preaveraging approximation is no longer valid for a system of high volume fraction.

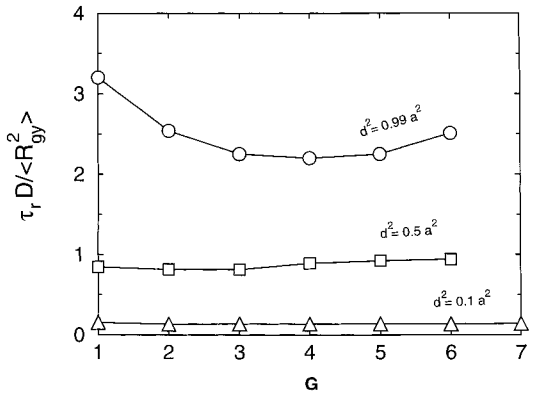

Figure 3. $\tau_r D/\langle R_{gy}^2 \rangle$ for our dendrimer models as a function of the total generation G. Circles, squares, and triangles represent systems with squared excluded-volume diameters $d^2 = 0.99a^2$, $0.5a^2$, and $d^2 = 0.1a^2$, respectively.

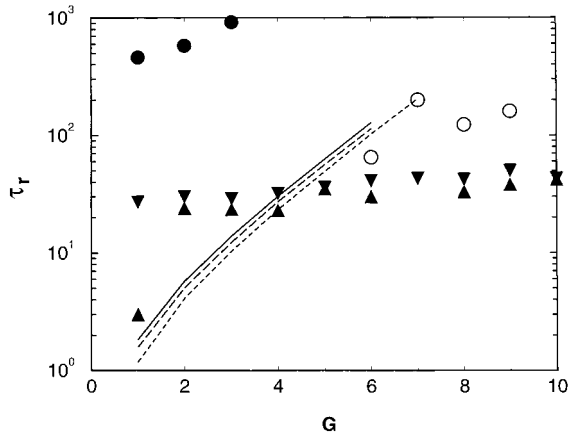

Figure 4. Dynamic relaxation times as a function of the total generation G. The solid, long-dashed, and dotted curves represent our calculation of τ_r listed in Table 1 for $d^2 = 0.99a^2$, $0.5a^2$, and $0.1a^2$. A constant $a^2\zeta/3k_BT$ has been used to rescale τ. The relaxation times for carbosilane dendrimers, determined by Stark et al., are represented by filled circles.[7] The relaxation times for PAMAM dendrimers, determined through measuring T_1 and T_2 in NMR experiments, are displayed by using filled down triangles (PAMAM at 23 °C) and filled up triangles (PAMAM at 25 °C). These experimental results are shown in 10^{-12} s. Also displayed on the figure are the relaxation times determined in a dendrimer molecular-dynamics (MD) simulation,[24] represented by open circles. Note that these results have been rescaled by a basic time unit in the MD simulation.

A comprehensive comparison between the relaxation times calculated here and experimental results relies on several other factors that are unknown to us. In Figure 4, we display the variation of τ_r as a function of G for various solvent qualities, represented by curves with various d^2. The filled circles represent experimental determination of relaxation times. Recently Stark et al. have performed a neutron scattering experiment[7] to probe the dynamic relaxation of carbosilane dendrimers up to $G = 3$. The relaxation times, corresponding to $G = 1-3$, are $\tau = 4{:}6,\ 5.8,\ 9.2 \times 10^{-10}$ s, which agree with the general increasing trend of our calculation; however, the increase is obviously much slower. Meltzer et al. have conducted deuterated NMR measurements of the spin−spin and spin−lattice relaxation times of PAMAM dendrimers.[2] The T_1 and T_2 results are then fitted to a formula that relates these NMR relaxation times to the dynamic relaxation times (called the

correlation times in these references). We have used filled triangles in Figure 4 to represent their τ in microseconds. The experimental results increase much slower than the results of our calculation of τ.

A direct measure of the autocorrelation functions in numerical experiments would shed some light on the behavior of the relaxation times. Murat and Grest have performed molecular-dynamics simulation for dendrimers up to eight generations (our nine generations).[24] However, the hydrodynamic interactions were not included in their computation. A truncated Lennard-Jones potential was applied to model the interaction between each pair of monomers, and a logarithm potential was used to account for the chemical bonding. The solvent condition was modeled by changing the temperature. We have used open circles in Figure 4 to represent their relaxation times for the athermal case. Their results also indicate a faster increase than that of the experimental data.

3. The Transport Coefficients

3.1. The Rouse and Zimm Approximations. In a Rouse approximation, one can easily show that the diffusion coefficient D is independent of the molecular structure and is always proportional to $(N+1)^{-1}$ where $N+1$ is the number of monomers in the model. The intrinsic viscosity $[\eta]$, however, depends on the architecture of the molecule. For linear polymers, $[\eta] \propto N$.[28] For dendrimers, we found that there is no simple scaling law between $[\eta]$ and G for small G, and $[\eta] \propto (G - 5/3)$ when G is large.[26]

The Zimm approximation qualitatively incorporates the physical features of both excluded volume and hydrodynamic interactions. For linear chains, $[\eta] \propto N^{3\nu-1}$ and $D \propto N^{-\nu}$ with $\nu = 0.5$ for the θ temperature and $\nu \approx 0.6$ for a good solvent. For dendrimers, computations of $[\eta]$ and D (listed below as η_Z and D_Z) can be performed with the preaveraging technique discussed in the previous section. However, we will show later that the preaveraging technique is a poor approximation for the intrinsic viscosity of dendrimers.

3.2. Fixman's Variational Bounds. The calculation of transport coefficients of macromolecules is a challenging task. In principle, molecular dynamics can be applied directly, but the computational demands far exceed the capability of modern computers. Instead of directly computing the exact value, Fixman has devised a method that can be used to estimate the upper and lower bounds from variations of trial functions, to sandwich the exact value. Since these bounds are directly expressed as equilibrium averages of some static quantities, Monte Carlo simulations can be used to perform the averages efficiently. Mathematically, Fixman's variational bounds are more rigorous than the Zimm preaveraging treatment, which totally disregards the correlation between the hydrodynamic interaction tensors and the coordinates. The derivation of the variational bounds can be found in Appendix B or in Fixman's original work.[34]

As discussed in Appendix B, the upper bound of the intrinsic viscosity reads[36]

$$\eta_U = \frac{\zeta}{\eta_s(N+1)} \sum_{jk} \langle \mathbf{u}^T \mathbf{H}^{-1} \mathbf{u} \rangle \tag{3.1}$$

and the lower bound

$$\eta_L = \frac{\zeta}{\eta_s(N+1)} \frac{\langle \mathbf{u}^T \langle \mathbf{H} \rangle^{-1} \mathbf{u} \rangle^2}{\langle \mathbf{u}^T \langle \mathbf{H} \rangle^{-1} \mathbf{H} \langle \mathbf{H} \rangle^{-1} \mathbf{u} \rangle} \tag{3.2}$$

where

$$\mathbf{u}_j = \frac{1}{2}(\hat{\mathbf{e}}_\alpha \hat{\mathbf{e}}_\beta + \hat{\mathbf{e}}_\beta \hat{\mathbf{e}}_\alpha) \cdot (\mathbf{r}_j - \mathbf{r}_C) \tag{3.3}$$

and $\mathbf{u} = (\mathbf{u}_0^T, ..., \mathbf{u}_N^T)^T$. These bounds slightly differ from Fixman's original proposal[34] where the reference center $\mathbf{r}_C$ is the the center of mass, not the drifting center used here. Similar expressions have been suggested by Mansfield and Klushin, and there the center of mass was also used.[27]

Under both Rouse and Zimm approximations, one writes $\mathbf{H}_{jk} = \langle \mathbf{H}_{jk} \rangle = H_{jk}\mathbf{I}$. Both upper and lower bounds now coincide with the intrinsic viscosity in a Zimm approximation,

$$\eta_Z = \eta_U = \eta_L = \frac{\zeta}{\eta_s(N+1)} \sum_{jk} \langle \mathbf{u}_j \cdot (H^{-1})_{jk} \mathbf{u}_k \rangle \tag{3.4}$$

Particularly, in the Rouse approximation, $H_{jk} = \delta_{jk}$, we have

$$\eta_R = \frac{\zeta}{6\eta_s} \langle R_{gy}^2 \rangle \tag{3.5}$$

which agrees with our previous discussion.[26]

There are various versions of the upper bounds for the diffusion constant D. The Kirkwood approximation,

$$D_K = \frac{k_B T}{(N+1)^2 \zeta} \sum_{jk} H_{jk} \tag{3.6}$$

for example, is known to be a higher estimate than the Zimm approximation,

$$D_Z = \frac{k_B T}{\zeta \sum_{jk} (H^{-1})_{jk}} \tag{3.7}$$

and both can be shown to be upper bounds (Appendix B). The lower bound,

$$D_L = \frac{k_B T}{\zeta \sum_{jk} \langle \hat{\mathbf{e}}_\gamma \cdot (\mathbf{H}^{-1})_{jk} \cdot \hat{\mathbf{e}}_\gamma \rangle} \tag{3.8}$$

involves the calculation of an average similar to that which appears in eq 3.1. In a preaveraging approximation where $\mathbf{H}_{jk} \equiv H_{jk}\mathbf{I}$, the lower bound coincides with the Zimm approximation in eq 3.7. All three expressions reduce to

$$D_R = \frac{k_B T}{(N+1)\zeta} \tag{3.9}$$

when $H_{jk} = \delta_{jk}$ in a Rouse approximation.

The calculations of η_Z, D_K and D_Z are relatively easy. One can perform Monte Carlo simulations to carry out the various averages involved in these expressions. The implementation of η_U and D_L in actual numerical computations, however, is time-consuming because one has to solve a system of $N_f = 3(N+1)$ linear equations

Table 2. Average and Maximal Iterations Used in the Gauss−Seidel Method when the Average in eq 3.1 Is Evaluated for Models with $d^2 = 0.99a^2$

G	av	max
1	4.7063	7
2	3.8487	7
3	3.2201	6
4	3.1088	5
5	3.5312	6
6	4.3533	7

Table 3. Comparison between the Performance of LU Decomposition Method (LU) and That of the Gauss−Seidel Method (GS) in Evaluating the Average in eq 3.1

G	$\mathbf{u}^T\mathbf{H}^{-1}\mathbf{u}$	LU method	GS method
1	ensemble average	0.170 31	0.170 22
2	ensemble average	0.286 20	0.286 85
3	ensemble average	0.381 21	0.382 61
4	ensemble average	0.449 39	0.450 80
5	sample no. 1	0.527 74	0.529 75
5	sample no. 2	0.478 22	0.478 82
5	sample no. 3	0.480 23	0.480 63
6	sample no. 1	0.539 06	0.536 49
6	sample no. 2	0.519 76	0.517 03
6	sample no. 3	0.534 79	0.531 97
6	sample no. 4	0.529 46	0.526 19

to obtain $\mathbf{H}^{-1}\mathbf{u}$ in every Monte Carlo step. For linear chains without excluded-volume interaction, Zimm computed the upper bounds, with Cholesky decomposition, up to 50 monomers.[20] A traditional method of linear system solving is LU decomposition, of which Cholesky decomposition is a special case. However, both Cholesky and LU decompositions are $N_f^3/3$ processes. When performed in each Monte Carlo step, the computation is almost impossible for large N_f. We thus resort to the Gauss−Seidel iteration method.[30,33] Since each iteration is now an N_f^2 process, the computational time can be greatly reduced, provided the series converges in very few iterations. For the numerical results presented below, we solved the equation $\mathbf{Hy} = \mathbf{u}$ with the Gauss−Seidel iteration method. We found that an initial approximation $\mathbf{y}^0 = \xi\langle\mathbf{H}\rangle\mathbf{u}$ with $0 < \xi < 1$ is a good guess. The optimal parameter ξ can be determined by trials for individual samples, and we used $\xi = 0.6$ for all computations. The series was considered to converge if the relative error of $\mathbf{u}^T\mathbf{H}^{-1}\mathbf{u}$ is less than 0.5% in two successive iterations. With such an initial condition, the series typically converges within five iterations. Table 2 gives a list of the maximal number and average number of iterations per Monte Carlo step. A comparison between the $\mathbf{u}^T\mathbf{H}^{-1}\mathbf{u}$ values determined from the LU decomposition method and the Gauss−Seidel iteration method is also shown in Table 3.

3.3. Numerical Results. To verify the validity of the numerical procedures, we have applied the technique to calculate the intrinsic viscosity of linear polymers with both hydrodynamic and excluded-volume interactions. In Figure 5, we show that all three approximations of $[\eta]$, given in eqs 3.1, 3.2, and 3.4 agree with each other rather well, even for the case of a strong excluded-volume interaction $d^2 = 0.99a^2$, up to a molecular weight $N = 200$. It is clear that the numerical results, represented by various symbols, obey the expected scaling law $[\eta] \propto N^{0.8}$. as can be inferred from the solid straight line that represents a slope of 0.8 (we have taken $\nu = 0.6$ here). Since the upper and lower bounds are so close to each other, the Zimm intrinsic viscosity can indeed be considered a good approximation of $[\eta]$ for linear

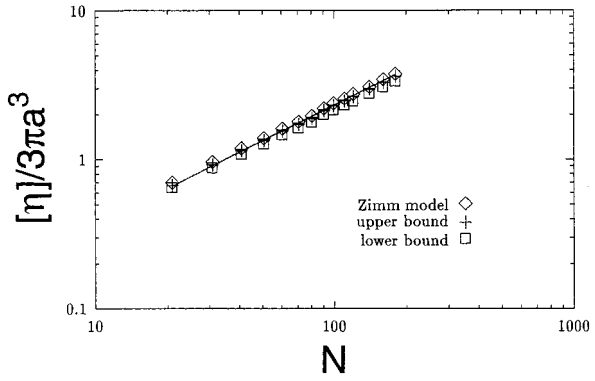

Figure 5. Comparison of various approximations in eqs 3.1 (crosses), 3.2 (squares), and 3.4 (diamonds) for the intrinsic viscosity of bead−bond linear polymers up to $N = 200$ units. An excluded-volume diameter of $0.99a$ has been used in generating these results. The solid line gives the slope expected by the scaling law. The three approximations agree with each other. Here, η is calculated in units of an inverse monomer weight.

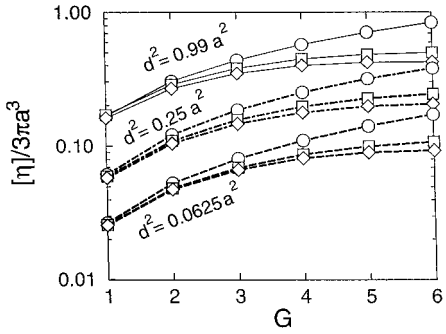

Figure 6. Comparison of various approximations in eqs 3.1 (squares), 3.2 (diamonds), and 3.4 (circles) for the intrinsic viscosity of the current dendrimer models up to $G = 6$ generations. Different solvent conditions are represented by various values of the squared excluded-volume diameters, $d^2 = 0.99a^2$, $0.25a^2$, and $0.0625a^2$. Two approximations (eqs 3.1 and 3.2) agree with each other, and the Zimm approximation (circles) disagrees with the expected value sandwiched between the squares and the diamonds at high G (in the high-volume fraction region).

Table 4. Reduced Intrinsic Viscosity $[\eta]/3\pi a^3$ [a]

G	η_Z	η_U	η_L
1	0.166 85	0.170 22	0.161 47
2	0.303 90	0.286 85	0.267 40
3	0.440 92	0.382 61	0.349 39
4	0.579 42	0.450 80	0.402 55
5	0.714 66	0.485 31	0.424 10
6	0.847 63	0.501 59	0.426 74

[a] Estimated by using the Zimm approximation and the variational methods, for the dendrimer models with $d^2 = 0.99a^2$.[36]

polymers. As eqs 3.1 and 3.4 demonstrate, the difference between η_Z and η_U lies in the correlation between $\mathbf{H}$ and the $\mathbf{u}_j\mathbf{u}_k$ tensors. For linear polymers, we have observed very little correlation numerically between these two tensors, which is possible when the involved volume fraction is low. However, as we find in the rest of this section, the situation changes dramatically for dendrimers, when the volume fraction starts to increase.

Displayed in Figure 6 is the intrinsic viscosity for dendrimers determined by the three approximations in eqs 3.1, 3.2, and 3.4. Various solvent conditions, represented by the excluded-volume diameters, were considered in all cases (see also Table 4). From these curves, one can conclude that Fixman's upper and lower bounds

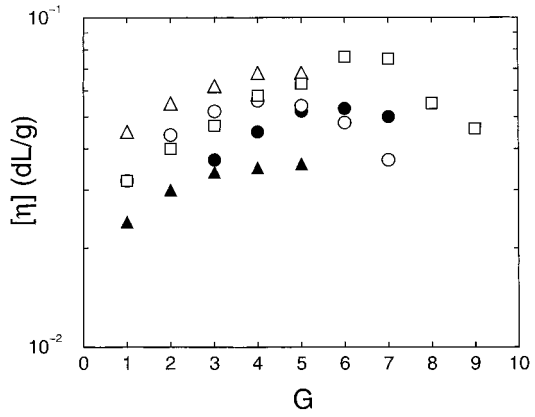

Figure 7. Experimental determination of the intrinsic viscosity of PAMAM (squares), polyether (open circles for tridendrons and filled circles for monodendrons), and poly(propyleneimine) [filled triangles for DAB−dendr−$(CN)_x$ and open triangles for DAB−dendr−$(NH_2)_x$]. Note that the intrinsic viscosity goes through a maximum in two cases. A recent diamond-lattice calculation of $[\eta]$ by Mansfield displays a similar maximum.[37] The theoretical calculation displayed in Figure 6 failed to explain such maxima. A revision of the current model to account for the difference in the diameter parameters appearing in the hydrodynamic and excluded-volume interactions gives rise to a maximum.[38]

(squares and diamonds) agree with each other even in the high-density regime at high G. The "real" value should be bracketed between these two bounds. The Zimm approximation (circles), however, yields a poor representation of the intrinsic viscosity in the high-density regime.

Experimental results for PAMAMs (squares), polyethers (open circles for tridendrons and filled circles for monodendrons), DAB−dendr−$(NH_2)_x$ (open triangles) and DAB−dendr−$(CN)_x$ (filled triangles) are plotted in Figure 7. One noticeable feature is the existence of maxima in some of these curves. These maxima have been the focus of some recent discussions. The kinetic simulation of a standard bead−bond model has yielded an interesting range for values for $[\eta]$, with a hint of a maximum in the $[\eta]$ curve.[27] A recent diamond lattice simulation by Mansfield for dendrimers up to $G = 9$, which incorporated the capacitance-viscosity mapping (a new technique for approximating the intrinsic viscosity), has yielded a peak similar to the experimental result.[37] Here, our calculation of the standard bead−bond model in free space does not produce the anticipated maximum, even for the strong excluded-volume case ($d^2 = 0.99a^2$). In a recent publication, we have discussed a possible revision to the standard bead−bond model, in which the excluded-volume diameter in the hydrodynamic matrix and in the interaction potential are treated differently. Maxima in $[\eta]$ are observed even for low generations.[38] Since DAB−dendr−$(NH_2)_x$ (open triangles) and DAB−dendr−$(CN)_x$ are based on two dendrons branching from the central core, the volume fractions of these systems are relatively low. Thus, $[\eta]$ cannot reached the crossover point where the volume fraction begin to dramatically increase, resulting a decrease in the $[\eta]$ curve.

The numerical results of the diffusion coefficients for dendrimers up to $G = 6$ under the Kirkwood (eq 3.6), Zimm (eq 3.7) and lower-bound (eq 3.8) approximations are displayed in Table 5 for $d^2 = 0.99a^2$. The computation of D_L is most computationally expensive and is implemented with the Gauss−Seidel iteration method

Table 5. Diffusion Coefficient D^a

G	D_L (lower bound)	D_Z (upper bound)	D_K (upper bound)
1	0.53952	0.55137	0.56284
2	0.34985	0.36472	0.38232
3	0.24481	0.26025	0.27798
4	0.18197	0.19526	0.21107
5	0.14073	0.15183	0.16509
6	0.11117	0.12111	0.13224
7	not available	0.09924	0.11172

[a] Estimated by using the variational methods for our dendrimer models with $d^2 = 0.99a^2$. D is expressed in units of k_BT/ζ.

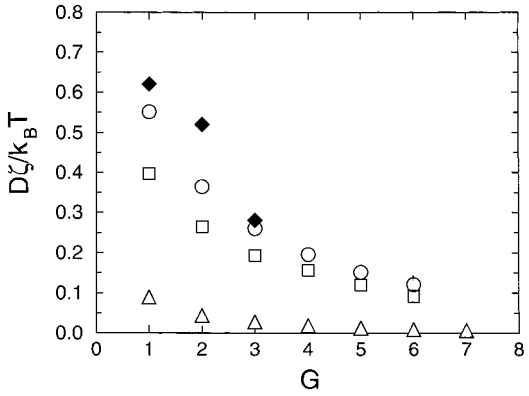

Figure 8. Diffusion coefficient of the current dendrimer models up to $G = 6$ generations for $d^2 = 0.99a^2$ (circles), $0.5a^2$ (diamonds), and $0.1a^2$ (squares). The Zimm approximation has been used to generate these data points. The variation of D represented by upper and low bounds is approximately the size of the circles used for $d^2 = 0.99a^2$. In addition, see Table 5 for a comparison between the three approximations, which agree with each other even in the high-volume fraction regime. Stark et al.'s determination of the diffusion constant based on quasielastic neutron scattering is also displayed by the filled circles, in 10^{-12} m^2/s.

as well. Clearly, the Zimm approximation (circles in Figure 8), as a variational upper bound, gives a very good approximation to the "true" D. The differences in the Kirkwood and lower-bound approximations are also displayed in in Table 5. Viewing the complication involved in evaluating D_L, the Zimm approximation is probably the simplest choice for the actual calculation. The other curves in Figure 8 are based on the Zimm approximation only.

Overlaying on Figure 8 are the diffusion coefficients (filled diamonds) measured by Stark et al. recently, where D of the first three generations of carbosilane dendrimers were measured through a quasielastic dynamic scattering.[7] The experimental D curve, determined from only three points, varies much faster then our theoretical predictions. It is unclear whether this is related to the distinct curvature of their relaxation time determinations (Figure 4, filled circles).

4. Summary

In this work, we systematically analyzed different theoretical techniques that can be used to calculate the dynamical properties of starburst dendrimers: the Zimm preaveraging and the Fixman variational-bound techniques. Equilibrium pivot Monte Carlo simulations have been used to evaluate various resulting thermodynamic averages. A free-space, bead−bond model (Figure 1) is used for all calculations.

From an analysis of the Langevin dynamics including hydrodynamic and excluded-volume interactions, we have concluded that (a) the normal modes, their eigenvalues, and their degeneracies share the same types of classification as in a Rouse approximation where none of the above-mentioned interactions are present (Figure 2); (b) a drifting mode, rather than the center of mass, should be considered in the presence of the hydrodynamic interaction (section 2.4); and (c) the relaxation times determined in this work qualitatively vary faster than the experimental determination of the correlation times of PAMAM dendrimers (Figure 4).

We have also applied the variational-bound technique to the estimation of the intrinsic viscosity and the diffusion coefficient. We found that (a) the Zimm approximation gives a rather poor estimate of the intrinsic viscosity at high volume fractions (Figure 6), (b) Fixman's upper and lower bounds are good approximations to the "real" intrinsic viscosity value, even for high-volume densities (Figure 6), (c) there is no maximum in the intrinsic viscosity curve up to $G = 6$ generations in the current model (Figure 6), and (d) all three approximations to the diffusion constants agree (Table 5).

Although we have used the standard bead−bond model in all of the calculations, improvements of the calculation are possible through the evaluation of the averages using more realistic intramolecular potentials.

We acknowledge the financial support of the Natural Sciences and Engineering Research Council of Canada and the help of S. W. Dwyer in proofreading this manuscript.

Appendix A: Eigenproblem in the Langevin Equation

When $\mathbf{H}_{jk} = H_{jk}\mathbf{I}$ and $U = {}^{K}/_{2}\sum_{jk}\mathbf{r}_j\cdot A_{jk}\mathbf{r}_k$, we only need to consider one of the three components in a Cartesian space

$$\frac{\mathrm{d}}{\mathrm{d}t}r = \frac{1}{\zeta}H(-KAr + f) \tag{A.1}$$

where the subscripts of the vectors have been dropped. The corresponding cummulants for the random forces become

$$\langle f\rangle = 0 \tag{A.2}$$

$$\langle f(t)f^{\mathrm{T}}(t')\rangle = 2k_{\mathrm{B}}T\zeta H^{-1}\delta(t - t') \tag{A.3}$$

Equation A.1 can be re-casted into a more convenient form,

$$H^{-1/2}\frac{\mathrm{d}}{\mathrm{d}t}r = -\frac{K}{\zeta}H^{1/2}AH^{1/2}H^{-1/2}r + \frac{1}{\zeta}H^{1/2}f \tag{A.4}$$

where $H^{1/2}$ is the square root of H. Now, the matrix $H^{1/2}AH^{1/2}$ is symmetric; so there exists an orthogonal matrix P such that $P^{\mathrm{T}}H^{1/2}AH^{1/2}P = \Lambda = \mathrm{diag}(\lambda_0, \lambda_1, ..., \lambda_N)$. Denoting $V = H^{1/2}P$, we can also make a transformation on the coordinates: $x = V^{-1}r$. Then eq A.1 reads

$$\frac{\mathrm{d}}{\mathrm{d}t}x = -\frac{K}{\zeta}\Lambda x + \frac{1}{\zeta}f' \tag{A.5}$$

where $f' = V^{-1}f = P^{\mathrm{T}}H^{-1/2}f$ and the first two cumulants of f' are

$$\langle f'\rangle = 0 \tag{A.6}$$

$$\langle f'(t)f'^{\mathrm{T}}(t')\rangle = 2k_{\mathrm{B}}T\zeta\delta(t - t') \tag{A.7}$$

Now, all the variables have been separated, and we only need to deal with a group of one-variable linear Langevin equations.

Appendix B: Variation Bounds for the Transport Coefficients

In this appendix, we outline the main steps of the derivation of the variational bounds. Let us consider an imposed external velocity field

$$\mathbf{V} = \kappa\hat{\mathbf{e}}_\alpha\hat{\mathbf{e}}_\beta\cdot\mathbf{r} \tag{B.1}$$

on $N + 1$ monomers, where κ is the shear rate. The velocity of the jth monomer is expressed as

$$\mathbf{v}_j = \mathbf{V}_j + \frac{1}{\zeta}\sum_k \mathbf{H}_{jk}\cdot\nabla_k U \tag{B.2}$$

The Smoluchowski equation for the stationary-state distribution function ψ then reads

$$\frac{1}{\zeta}\sum_{jk}\nabla_j\cdot\mathbf{H}_{jk}\cdot(k_{\mathrm{B}}T\nabla_k\psi + \psi\nabla_k U) - \sum_j\nabla_j\cdot(\mathbf{V}_j\psi) = 0 \tag{B.3}$$

One can express the relative increment in viscosity in terms of a nonequilibrium average[28,36]

$$[\eta] = \frac{1}{\eta_s(N+1)}\lim_{\kappa\to 0}\frac{1}{\kappa}\sum_j\langle\nabla_j U\cdot\hat{\mathbf{e}}_\alpha\hat{\mathbf{e}}_\beta\cdot\mathbf{r}_j\rangle_{ne} \tag{B.4}$$

Letting $\psi = \Phi\psi_{\mathrm{eq}}$, where ψ_{eq} is the equilibrium distribution function and $\Phi = 1 + O(\kappa)$ satisfies $\sum_j\nabla_j\Phi = 0$, we can rewrite eq B.3

$$1/\zeta\sum_{jk}\nabla_j\cdot(k_{\mathrm{B}}T\psi_{\mathrm{eq}}\mathbf{H}_{jk}\cdot\nabla_k\Phi) = \sum_j\nabla_j\cdot(\mathbf{V}_j\psi_{\mathrm{eq}}) \tag{B.5}$$

where the right-hand side is a term accurate to linear order in κ. Since $\psi_{\mathrm{eq}} = \exp(-U/K_{\mathrm{B}}T)$ and $\nabla_j\cdot V_j = 0$, the average in eq B.4 becomes

$$\langle\nabla_j U\cdot\hat{\mathbf{e}}_\alpha\hat{\mathbf{e}}_\beta\cdot\mathbf{r}_j\rangle_{ne} = \frac{k_{\mathrm{B}}T}{\kappa}\langle\mathbf{V}_j\cdot\nabla_j\Phi\rangle \tag{B.6}$$

Integrating eq B.5, we obtain

$$\frac{k_{\mathrm{B}}T}{\zeta}\nabla_k\Phi = \sum_j(\mathbf{H}^{-1})_{kj}\cdot(\mathbf{V}_j + \mathbf{V}_j^{(0)}) \tag{B.7}$$

where $\mathbf{V}^{(0)}_{0,...,N}$ serve as integral constants and must satisfy $\sum_j\nabla_j\cdot(\mathbf{V}_j^{(0)}\psi_{\mathrm{eq}}) = 0$. The intrinsic viscosity can thus be written as

$$[\eta] = \frac{\zeta}{\eta_s\kappa^2(N+1)}\sum_{jk}\langle(\mathbf{V}_j + \mathbf{V}_j^{(0)})\cdot(\mathbf{H}^{-1})_{jk}\cdot(\mathbf{V}_k + \mathbf{V}_k^{(0)})\rangle \tag{B.8}$$

We can now show that since $\mathbf{H}^{-1}$ is positive definite, the quadric form inside the summation guarantees that using any trial function to replace $V^{(0)}$ will yield a value

greater then the actual one. One logical choice will be to use

$$\mathbf{V}_j^{(0)} = -\kappa \hat{\mathbf{e}}_\alpha \hat{\mathbf{e}}_\beta \cdot \mathbf{r}_C + \frac{\kappa}{2} \hat{\mathbf{e}}_\gamma (\mathbf{r}_j - \mathbf{r}_C) \tag{B.9}$$

where $\mathbf{r}_C$ is the drifting center in eq 2.17, which retains the most important symmetry properties of the system. Therefore, we arrive at the upper bound in eq 3.1.

To obtain the lower bound, we consider an arbitrary function $\Phi^* = \Phi + \delta\Phi$ satisfying $\sum_j \nabla_j \Phi^* = 0$. Multiplying both sides of eq B.5 by Φ^* and then integrating both sides, we have

$$\frac{k_B T}{\zeta} \sum_{jk} \langle \nabla_j \Phi^* \cdot \mathbf{H}_{jk} \cdot \nabla_k \Phi \rangle = \sum_j \langle \mathbf{V}_j \cdot \nabla_j \Phi^* \rangle \tag{B.10}$$

Thus,

$$\begin{aligned} \sum_j \langle \mathbf{V}_j \cdot \nabla_j \Phi \rangle &= \frac{k_B T}{\zeta} \sum_{jk} \langle \nabla_j \Phi \cdot \mathbf{H}_{jk} \cdot \nabla_k \Phi \rangle \\ &= -\frac{k_B T}{\zeta} \sum_{jk} \langle \nabla_j \Phi^* \cdot \mathbf{H}_{jk} \cdot \nabla_k \Phi^* \rangle + \\ &\quad 2 \sum_j \langle \mathbf{V}_j \cdot \nabla_j \Phi^* \rangle + \frac{k_B T}{\zeta} \sum_{jk} \langle \nabla_j \delta\Phi \cdot \mathbf{H}_{jk} \cdot \nabla_k \delta\Phi \rangle \\ &\geq -\frac{k_B T}{\zeta} \sum_{jk} \langle \nabla_j \Phi^* \cdot \mathbf{H}_{jk} \cdot \nabla_k \Phi^* \rangle + \\ &\quad 2 \sum_j \langle \mathbf{V}_j \cdot \nabla_j \Phi^* \rangle \end{aligned} \tag{B.11}$$

Choosing the trial function $\Phi^* = 1 + \xi \sum_{jk} (r_{j\alpha} - r_{C\alpha})(H^{-1})_{jk}(r_{k\beta} - r_{C\beta})$ and then maximizing the lower bound with respect to ξ, we obtain the lower bound in eq 3.2.

Next, we consider the derivation of the variational bounds for D. In a weak external force field $\mathbf{F} = F\hat{\mathbf{e}}_\gamma$, the center of mass of each molecule will drift with a constant velocity $\mathbf{V}_C = V_C \hat{\mathbf{e}}_\gamma$ at a steady state. The velocity of the jth monomer is

$$\mathbf{v}_j = \frac{1}{\zeta} \sum_k \mathbf{H}_{jk} \cdot (-\nabla_k U + \mathbf{F}) \tag{B.12}$$

thus

$$\mathbf{V}_C = \frac{1}{(N+1)\zeta} \sum_{jk} \mathbf{H}_{jk} \cdot \left(\frac{k_B T}{\psi_{eq}} \nabla_k \psi_{eq} + F \hat{\mathbf{e}}_\gamma \right) \tag{B.13}$$

The diffusion coefficient measures the average of this velocity and is defined to be

$$D = \frac{k_B T}{(N+1)} \lim_{F \to 0} \frac{\langle V_C \rangle_{ne}}{F} \tag{B.14}$$

where

$$\begin{aligned} \langle V_C \rangle_{ne} &= \frac{F}{(N+1)\zeta} \sum_{jk} \langle \hat{\mathbf{e}}_\gamma \cdot \mathbf{H}_{jk} \cdot \hat{\mathbf{e}}_\gamma \rangle_{ne} + \\ &\quad \frac{k_B T}{(N+1)\zeta} \sum_{jk} \int \mathrm{d}x \, \hat{\mathbf{e}}_\gamma \cdot \mathbf{H}_{jk} \cdot \Phi \nabla_k \psi_{eq} \\ &= \frac{F}{(N+1)\zeta} \sum_{jk} \langle \hat{\mathbf{e}}_\gamma \cdot \mathbf{H}_{jk} \cdot \hat{\mathbf{e}}_\gamma \rangle - \\ &\quad \sum_k \frac{k_B T}{(N+1)F} \langle \mathbf{V}_k \cdot \nabla_k \Phi \rangle \end{aligned} \tag{B.15}$$

accurate up to linear order in F. The diffusion coefficient is thus

$$\begin{aligned} D &= \frac{k_B T}{(N+1)^2 \zeta} \sum_{jk} \langle \hat{\mathbf{e}}_\gamma \cdot \mathbf{H}_{jk} \cdot \hat{\mathbf{e}}_\gamma \rangle - \\ &\quad \lim_{F \to 0} \frac{k_B^2 T^2}{(N+1)^2 F^2} \sum_k \langle \mathbf{V}_k \cdot \nabla_k \Phi \rangle \end{aligned} \tag{B.16}$$

where the second term is similar to the expression in eq B.6 for the intrinsic viscosity.

The same procedure can thus be followed in analyzing the second term. The upper bound of D is related to the lower bound of $[\eta]$,

$$\begin{aligned} D_U &= D_K + \frac{k_B^3 T^3}{(N+1)^2 F^2 \zeta} \sum_{jk} \langle \nabla_j \Phi^* \cdot \mathbf{H}_{jk} \cdot \nabla_k \Phi^* \rangle - \\ &\quad \frac{2 k_B^2 T^2}{(N+1)^2 F \zeta} \sum_{jk} \langle \hat{\mathbf{e}}_\gamma \cdot \mathbf{H}_{jk} \cdot \nabla_k \Phi^* \rangle \end{aligned} \tag{B.17}$$

where Φ^* is an arbitrary function satisfying $\sum_j \nabla_j \Phi^* = 0$. As a most crude approximation, one can let $\Phi \equiv 1$, which results in the Kirkwood upper bound of the diffusion equation in eq 3.6.[15] A better estimate for the upper bound can be found by defining $\Phi = 1 + \sum_j c_j r_{j\gamma}$, where $\sum_j c_j = 0$, and by minimizing the upper bound within this constraint. This improved upper bound is displayed in eq 3.7 and actually coincides with the expression of the diffusion constant in a Zimm approximation. The variational lower bound of D is related to eq B.8,

$$D \geq D_K - \frac{k_B T \zeta}{N^2 F^2} \sum_{jk} \langle (\mathbf{V}_j + \mathbf{V}_j^{(0)}) \cdot (\mathbf{H}^{-1})_{jk} \cdot (\mathbf{V}_k + \mathbf{V}_k^{(0)}) \rangle \tag{B.18}$$

The simplest choice of the velocity field is $\mathbf{V}_k \equiv c\hat{\mathbf{e}}_\gamma$. Maximizing the lower bound with respect to c, we find the appropriate lower bound displayed in eq 3.8.

References and Notes

(1) Tomalia, D. A.; Baker, H.; Dewald, J.; Hall, M.; Kallos, G.; Martin, S.; Roeck, J.; Ryder, J.; Smith, P. *Polym. J.* **1985**, *17*, 117. Tomalia, D. A.; Baker, H.; Dewald, J.; Hall, M.; Kallos, G.; Martin, S.; Roeck, J.; Ryder, J.; Smith, P. *Macromolecules* **1986**, *19*, 2466. Tomalia, D. A.; Naylor, A. M.; Goddard, W. A., III. *Angew. Chem. Int. Ed. Engl.* **1990**, *29*, 138. Tomalia, D. A.; Hedstrand, D. M.; Wilson, L. R. *Encyclopedia Polymer Science and Engineering*, 2nd Ed.;

Wiley: New York, 1990. Moreno-Bondi, M. C.; Orellana, G.; Turro, N. J.; Tomalia, D. A. *Macromolecules* **1990**, *23*, 912.
(2) Meltzer, A. D.; Tirrell, D. A.; Jones, A. A.; Inglefield, P. T.; Hedstrand, D. M.; Tomalia, D. A. *Macromolecules* **1992**, *25*, 4541. Meltzer, A. D.; Tirrell, D. A.; Jones, A. A.; Inglefield, P. T. *Macromolecules* **1992**, *25*, 4549.
(3) Hawker, C. J.; Fréchet, J. M. J. *J. Chem. Soc., Chem. Commun.* **1990**, *15*, 1010; *J. Am. Chem. Soc.* **1990**, *112*, 7638; *Macromolecules* **1990**, *23*, 4726.
(4) Newkome, G. R.; Lin, X. *Macromolecules* **1991**, *24*, 1443. Morikawa, A.; Kamimoto, M.; Imai, Y. *Macromolecules* **1991**, *24*, 3469.
(5) Mourey, T. H.; Turner, S. R.; Rubinstein, M.; Fréchet, J. M. J.; Hawker, C. J.; Wooley, K. L. *Macromolecules* **1992**, *25*, 2401. Fréchet, J. M. J. *Science* **1994**, *263*, 1710.
(6) Scherrenberg, R.; Coussens, B.; van Vliet, P.; Edouard, G.; Brackman, J.; de Brabander, E.; Mortensen, K. *Macromolecules* **1998**, *31*, 456.
(7) Stark, B.; Stühn, B.; Frey, H.; Lach, C.; Lorenz, K.; Frick, B. *Macromolecules* **1998**, *31*, 5415.
(8) Welch, P.; Muthukumar, M. *Macromolecules* **1998**, *31*, 5892.
(9) de Gennes, P. G.; Hervet, H. *J. Phys. (Paris)* **1983**, *44*, L351.
(10) Lescanec, R. L.; Muthukumar, M. *Macromolecules* **1990**, *23*, 2280.
(11) Mansfield, M. L.; Klushin, L. I. *Macromolecules* **1993**, *26*, 4262.
(12) Chen, Z. Y.; Cui, S.-M. *Macromolecules* **1996**, *29*, 7943.
(13) Boris, D.; Rubinstein, M. *Macromolecules* **1996**, *29*, 7251.
(14) Duplantier, B. *J. Stat. Phys.* **1989**, *54*, 581.
(15) Kirkwood, J. G.; Riseman, J. *J. Chem. Phys.* **1948**, *16*, 565. Kirkwood, J. G. *J. Polym. Sci.* **1954**, *12*, 1.
(16) Rouse, P. E. *J. Chem. Phys.* **1953**, *21*, 1272.
(17) Zimm, B. H. *J. Chem. Phys.* **1956**, *24*, 269.
(18) Zimm, B. H.; Kilb, R. W. *J. Polym. Sci.* **1959**, *37*, 19.
(19) Ermak, D. L.; McCammon, J. A. *J. Chem. Phys.* **1978**, *69*, 1352.
(20) Zimm, B. H. *Macromolecules* **1980**, *13*, 592.
(21) Fixman, M. *Macromolecules* **1981**, *14*, 1710; *J. Chem. Phys.* **1986**, *84*, 4085.
(22) Binder, K. *Monte Carlo and Molecular Dynamics Simulations in Polymer Science*; Oxford University Press: New York, 1995.
(23) Naylor, A. M.; Goddard, W. A., III; Kiefer, G. E.; Tomalia, D. A. *J. Am. Chem. Soc.* **1989**, *111*, 2339.
(24) Murat, M.; Grest, G. S. *Macromolecules* **1996**, *29*, 1278.
(25) La Ferla, R. *J. Chem. Phys.* **1997**, *106*, 688.
(26) Cai, C.; Chen, Z. Y. *Macromolecules* **1997**, *30*, 5104.
(27) Mansfield, M. L.; Klushin, L. I. *J. Phys. Chem.* **1992**, *96*, 3994.
(28) Doi, M.; Edwards, S. F. *The Theory of Polymer Dynamics*; Clarendon Press: 1994.
(29) Rotne, J.; Prager, S. *J. Chem. Phys.* **1969**, *50*, 4831.
(30) Barnett, S. *Matrices: Methods and Applications*; Clarendon Press: 1990.
(31) Press, W. H.; Flannery, B. P.; Teukolsky, S. A.; Vetterling, W. T. *Numerical Recipes: the Art of Scientific Computing (FORTRAN Version)*; Cambridge University Press: New York, 1992.
(32) Cai, C. M. Sc. Thesis, University of Waterloo, 1997.
(33) Sewell, G. *Computational Methods of Linear Algebra*; Ellis Horwood: New York, 1990.
(34) Fixman, M. *J. Chem. Phys.* **1983**, *78*, 1588.
(35) Grest, G. S.; Kremer, K.; Milner, S. T.; Witten, T. A. *Macromolecules* **1989**, *22*, 1904.
(36) Here, the denominator is written as $N+1$ instead of M where M is the molecular weight of a dendrimer.[28] Therefore, η's in eqs 3.1−3.5 and B.4 and B.8 are all written in units of inverse monomer weight.
(37) Mansfield, M. L. *Macromolecules*, in press.
(38) Cai, C.; Chen, Z. Y. *Macromolecules* **1998**, *31*, 6393.

MA990018Y